DC Smart
www.dcsmart.eu

Results of the smart grid control strategies in demonstration site

Version 1

Deliverable 6.2

Pierre-Jean Alet, Nelson Koch

31 March 2019

ERA-Net Smart Grids Plus | From local trials towards a European Knowledge Community

This project has received funding in the framework of the joint programming initiative ERA-Net Smart Grids Plus, with support from the European Union's Horizon 2020 research and innovation programme.

Smart Grids Plus
ERA-Net

INTERNAL REFERENCE

- **Deliverable No.:** D 6.2
- **Deliverable Name:** Results of the smart grid strategy in the demonstration site
- **Lead Partner:** CSEM
- **Work Package No.:** 6
- **Task No. & Name:** 6.3 Experiences and good practice
- **Document (File):** DCSMART_PJA_D6p2.docx
- **Issue (Save) Date:** 2019-03-31

DOCUMENT SENSITIVITY

☐	**Not Sensitive**	Contains only factual or background information; contains no new or additional analysis, recommendations or policy-relevant statements
☒	**Moderately Sensitive**	Contains some analysis or interpretation of results; contains no recommendations or policy-relevant statements
☐	**Sensitive**	Contains analysis or interpretation of results with policy-relevance and/or recommendations or policy-relevant statements
☐	**Highly Sensitive Confidential**	Contains significant analysis or interpretation of results with major policy-relevance or implications, contains extensive recommendations or policy-relevant statements, and/or contain policy-prescriptive statements. This sensitivity requires SB decision.

DOCUMENT STATUS

	Date	Person(s)	Organisation
Author(s)	29/03/2019	Pierre-Jean Alet, Nelson Koch	CSEM
Verification by			
Approval by			

CONTENTS

Disclaimer

The content and views expressed in this material are those of the authors and do not necessarily reflect the views or opinion of the ERA-Net SG+ initiative. Any reference given does not necessarily imply the endorsement by ERA-Net SG+.

About ERA-Net Smart Grids Plus

ERA-Net Smart Grids Plus is an initiative of 21 European countries and regions. The vision for Smart Grids in Europe is to create an electric power system that integrates renewable energies and enables flexible consumer and production technologies. This can help to shape an electricity grid with a high security of supply, coupled with low greenhouse gas emissions, at an affordable price. Our aim is to support the development of the technologies, market designs and customer adoptions that are necessary to reach this goal. The initiative is providing a hub for the collaboration of European member-states. It supports the coordination of funding partners, enabling joint funding of RDD projects. Beyond that ERA-Net SG+ builds up a knowledge community, involving key demo projects and experts from all over Europe, to organise the learning between projects and programs from the local level up to the European level.

www.eranet-smartgridsplus.eu

1. Introduction

The DCSMART project includes two demonstrators, one in the Netherlands and on in Switzerland. The purpose of the Swiss demonstrator is to validate, in an industrial environment, the smart grid control strategies developed by CSEM for a DC microgrid. These control strategies aim at providing services both to the public distribution system and to the end user. In this architecture, the end user benefits from an increased self-consumption in locally-produced electricity, the distribution system benefits from smoother power variations thanks to the limitation ramp rates, and both benefit from peak shaving. Indeed, there is a technical benefit for the distribution system which is already in current regulations passed on to end users in the form of the peak-power component of the electricity bill, as is common for commercial and industrial customers.

The site of the Swiss demonstrator was assessed in details in DCSMART's deliverable 6.1, which also includes a technical-economic analysis of the theoretical impact of the developed solution.

The purpose of this report is to assess the translation of the control strategies from theory to practice.

It is organised as follows:

- The first chapter provides a detailed description of the design and theoretical performance of the latest version of the control strategies
- The second chapter describes the additions that proved necessary to adapt to the physical limitations of the components in the demonstrator
- The third chapter describes the demonstrator as operational since December 2018
- The fourth chapter describes the data acquisition solution on the Swiss demonstration site
- The fifth chapter describes some minor outstanding technical issues
- The sixth chapter provides a detailed validation of each feature of the control strategy.

2. Control strategy: objectives, design and simulation

The control strategy developed by CSEM for the Swiss demonstration site aims at providing three smart grid services:

- Increase in local, self-consumption of locally-produced renewable electricity. This service is mainly of benefit to the end user (prosumer) who can thus reduce their electricity bill. When combined with other services it can also provide benefits to the wider distribution system since it reduces the load on the distribution network.
- Limitation of upward and downward ramp rates. This service is of benefit to the distribution system only. Indeed, it makes it easier for distribution system operators and other grid operators to operate their assets since it makes the grid more predictable. This feature is currently mandated by regulation in some island grids but in continental Europe there is no way to monetize it yet.
- Reduction in peak power. This service is of technical benefit to the distribution network operator, since reducing the peak load translates into reduced investment need. Thanks to the peak-power component of the electricity bill, which is commonly applied to commercial and industrial users, this service is also of economic benefit to the end user.

Figure 1 illustrates the topology of the implemented control strategy that is split in three different levels: the physical system, the first control level characterized by fast and simple controllers, and the supervision level where more advanced and slower control technics are used. More details about these levels are given below.

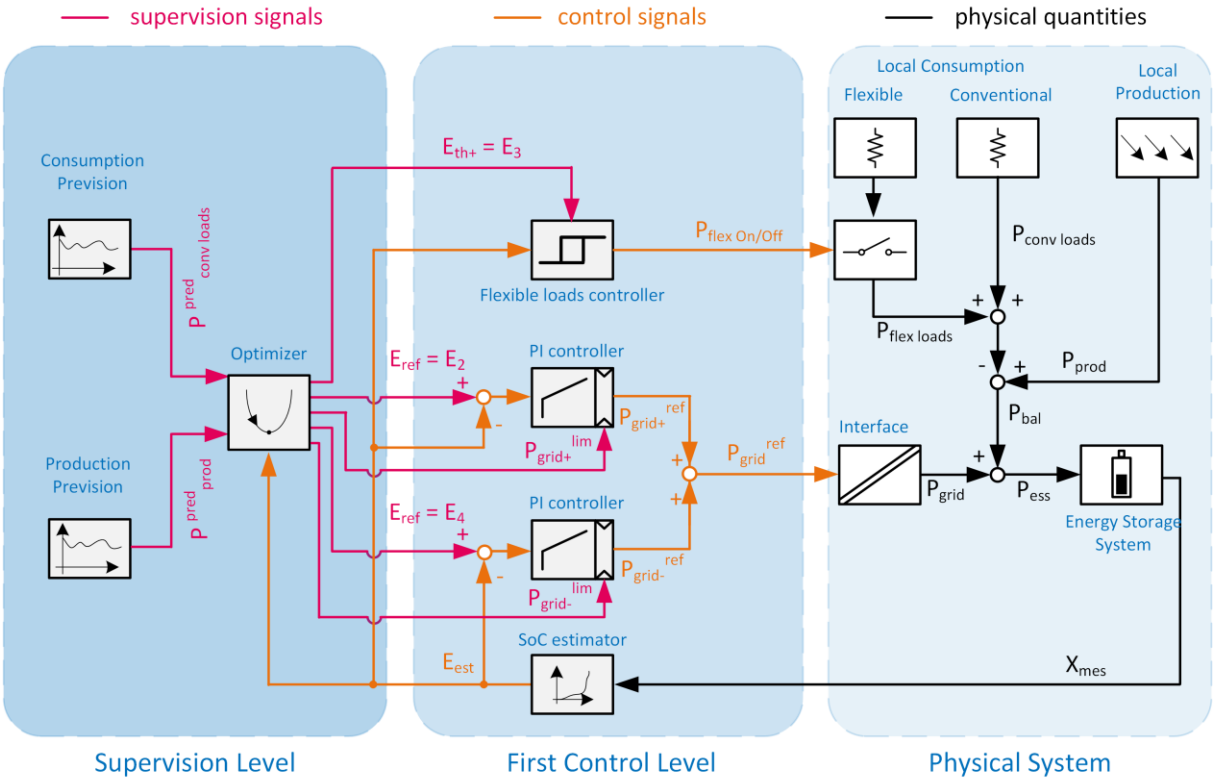

Figure 1: Layers and detailed implementation of the control strategy

On the lowermost level, the physical system, and as previously mentioned, the active and controllable elements are the AC/DC interface converter and the DC/DC converter supplying the flexible loads, here represented as a switch. The first one acts on the system by extracting power from or injecting power to the grid while the second can turn on or off the controllable loads.

These devices act on information coming from the first control level. There, the state of the complete system i.e. the SoC of the energy storage system, is estimated based on the DC-link voltage, assuming a bijective function linking these two values. This estimated SoC is compared to reference values to compute the error signal of two PI controllers the role of which is respectively to define the set-point for the power extracted from or injected into the AC grid. This estimation of the SoC is also compared to a third reference value in order to determine the state of the flexible loads.

These reference values can be fixed and predefined, during the system design for example, or continuously optimized based on previsions of the local production and consumption. These operations would occur at the supervision level, as illustrated on Figure 1.

2.1 PI controllers for the different services

The different energy services mentioned in the introduction of this document (increased self-consumption, peak-shaving and ramp-rate limitation) are provided through the adequate use of the two PI controllers illustrated on Figure 1. More details are given below for each of these services.

2.1.1 Self-consumption

The increased self-consumption is achieved by the use of unidirectional PI controllers with clearly separated reference values. One of the PI controller can only impose a positive reference value for the power exchanged with the grid i.e., a power extracted from the grid. Its reference SoC value, E_2, is lower than the reference value E_4, of the second PI controller that can only impose a negative reference value i.e., a power injected to the grid.

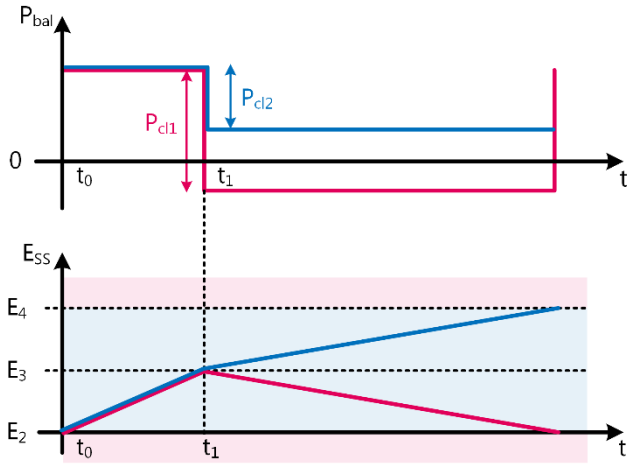

Figure 2: Evolution of the power balance and the battery state of charge in two scenarios

Between these two thresholds, no power is exchanged with the grid and the ESS SoC evolution depends on the internal power balance, as schematically illustrated on Figure 2.

If the local production exceeds the local consumption, the excess energy is stored in the Energy Storage System until this SoC reaches E_4 and the corresponding PI starts to inject the excess power into the grid to stabilize the SoC at its reference value. On the other hand, if the local consumption exceeds the local production, the required additional energy is taken out of the ESS, making its SoC decrease until the E_2 threshold is reached and the corresponding PI controller starts to take power from the grid to stabilize the SoC at this reference value.

Therefore, the energy storage capacity corresponding to the difference between these two thresholds is used to increase the self-consumption since it is used to momentarily store excess energy production in order to use it later when the local production is not enough to entirely supply the local consumption.

2.1.2 Peak shaving

The same PI controllers can also be used to provide the peak-shaving service, both for the power extracted from the grid and for the power injected into it. This is achieved by setting a limitation to the power reference value that is computed by the PI controllers. Figure 3 illustrates this behaviour for a limited injected power.

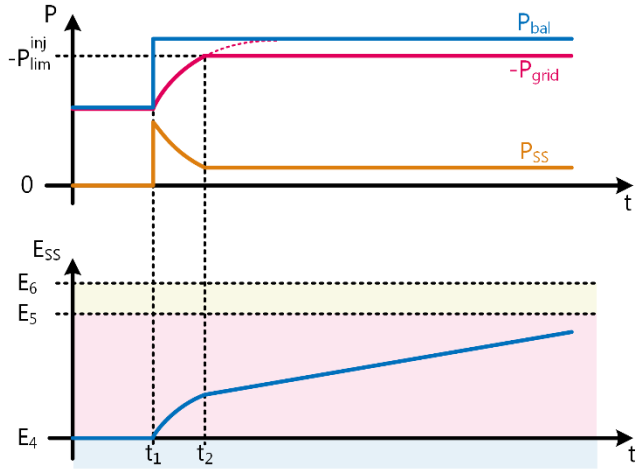

Figure 3: Evolution of the net power consumption (P_{bal}), the power exchanged with the grid (P_{grid}), the charge/discahrge power of the battery system (P_{ss}), and the state of charge of the storage system (E_{ss}) illustrating peak-shaving for the injected power.

Once the SoC is stabilized at E_4, if the local production still increases so that the power balance exceeds the set limitation, the reference value for the injected power will be limited and the remaining excess power will be then be stored in the ESS. For security reasons, this limitation is disabled when the SoC reaches the E_5 threshold. Thus, the energy storage capacity corresponding to the difference between E_4 and E_5 is used to provide the peak-shaving service. A similar reasoning can be done for the power extracted from the grid. In such a case, the corresponding storage capacity will be the one between E_1 and E_2.

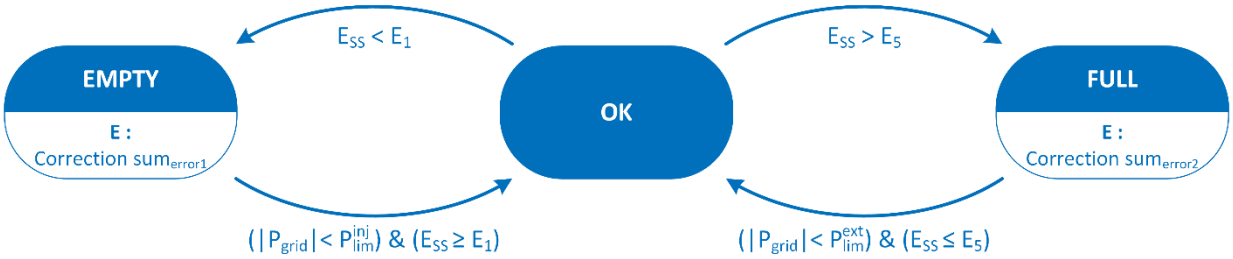

Figure 4: State machine controlling the peak-power limitation, which is activated when the system is in the central ("OK") state.

As previously mentioned, the power limitation can be disabled when the SoC reaches the E_1 and E_5 thresholds, respectively to avoid an excess charging and excess discharging of the energy storage system, as summarized on Figure 4.

In order to avoid a ringing phenomenon between the states where the power limitation is disabled and enabled, a second condition is added on the grid power reference value. This reference value must be, in absolute value, less than the limitation.

Moreover, it must also be noted that an artificial correction is performed on the PI controller internal state, the cumulated error, when the power limitation is disabled. This corrections allows to ensure a continuity in the power reference value computed by the PI controller.

2.1.3 Ramp-rate limitation

The last service, the ramp-rate limitation, is also performed thanks to the use of the PI controllers. More precisely, this service is achieved through the definition of the closed-loop equivalent time constant. Indeed, it can be mathematically demonstrated that the time constant characterizing the response of the PI controller to a perturbation is the

same that the time constant characterizing the response of the system to a change of reference value.

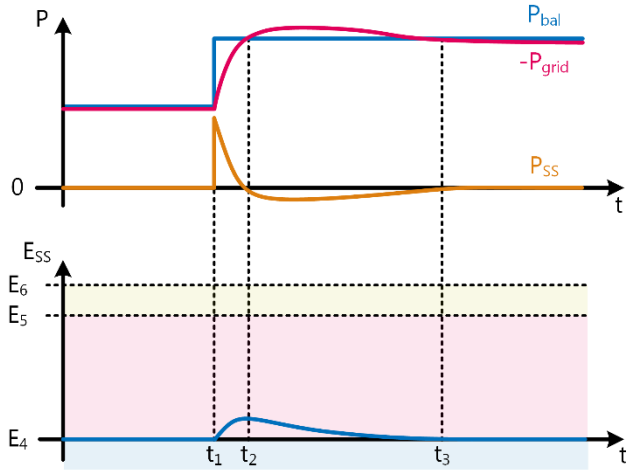

Figure 5: Evolution of the net power consumption (P_{bal}), the power exchanged with the grid (P_{grid}), the charge/discahrge power of the battery system (P_{ss}), and the state of charge of the storage system (E_{ss}) illustrating the limitation of grid power variations.

Figure 5 illustrates the limitation of the variation of grid power compared to the variation of the perturbation, here a suddenly increasing local production when the SoC is stabilized at E_4. In such a case, the sudden increase in the power balance will lead to an increasing SoC, thus creating an error from the PI controller point of view. The controller will react to this error and increase the power injected into the grid to bring the SoC back to its reference value. Nevertheless, the controller reacts with a limited and predefined bandwidth and therefore acts as a low-pass filter, effectively limiting the variation of the power exchanges with the grid. Such a behaviour is made possible by the fact that, during the transient, the power difference is assumed by the energy storage system, as depicted in orange on Figure 5, and lead to a transient increase of the SoC, reaching its maximum at $t=t_2$ on the considered figure. This maximal value is directly linked to the controller bandwidth and the magnitude of the perturbation. Thus, a security margin must be kept regarding the maximum and minimum allowed SoC. On Figure 5, this margin corresponds to the energy storage capacity located between E_5 and E_6. A similar reasoning can be made on the low-SoC side of the energy storage, with a security margin located between E_0 and E_1.

As previously mentioned, it can be demonstrated that the limitation of the ramp-rate is defined by the closed-loop bandwidth of the SoC control through the PI controller. This controller can be designed through the loop-shaping approach illustrated on Figure 6.

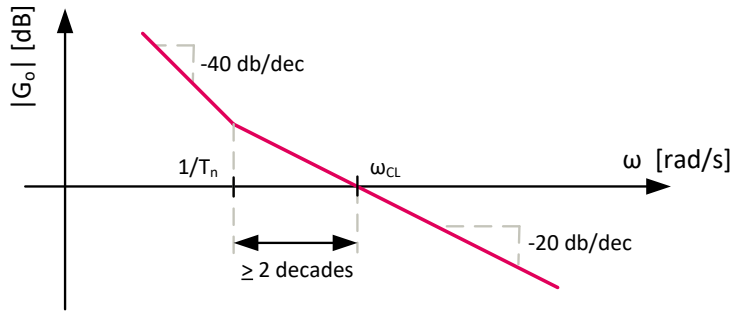

Figure 6: Sizing of the PI controller for a given closed-loop bandwidth

PI parameters T_n and T_i are adjusted such that the open-loop transfer function, given by the product of the transfer function of the controller and of the system, a pure integrator

in the considered case, crosses the 0db line at a pulsation ω_{cl} corresponding to the desired dynamic. Moreover, the change of slope, from -20db/decade to -40 db/decade must occur at least two decades away from the crossing of the 0db line.

Such a sizing of the PI controllers ensure a behaviour close enough to the first-order low-pass filter approximation mentioned above. It must be mentioned here that the two PI controllers can be sized with different bandwidth if the distinct dynamic behaviours are wished for the injected and extracted power.

2.2 Virtual splitting of the storage capacity

These considerations on the link between the different energy services and the parts of the energy storage capacity they use can be summarized according to Figure 7.

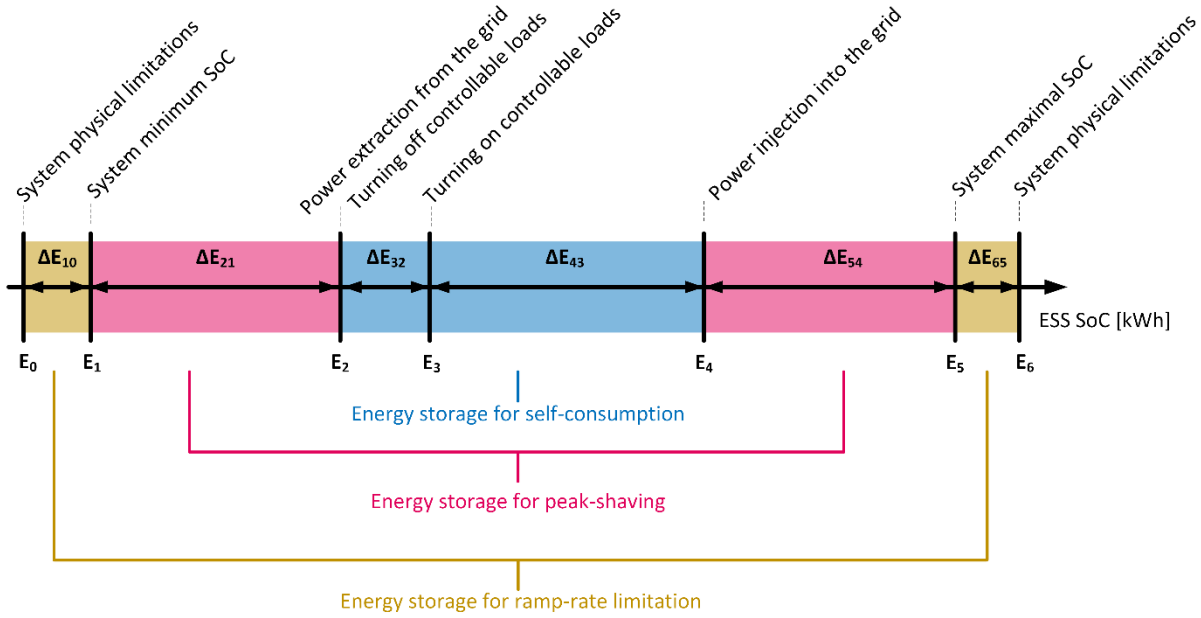

Figure 7: Allocation of storage capacity to the different services

The coloured areas correspond to the different energy services: yellow for the ramp-rate limitation, red for the peak-shaving and blue for the increased self-consumption. This last area includes an additional threshold, E_3, linked to the use of flexible loads. If the SoC reaches this value, the flexible loads will be turned on in order to increase the local consumption in order to bring the SoC back to E_2. In order to avoid ringing phenomena, an hysteresis is introduced and these flexible loads will not be turned off before the SoC reaches the lower bound of the area dedicated to self-consumption, namely E_2.

It must also be noted that ramp-rate limitation is also performed in the red areas. This detail is not mentioned on Figure 7 for the sake of simplicity.

3. Control strategy: practical implementation

While the control strategy described in section 2 has been validated in simulation, its practical translation on a physical system has required additional developments to account for the limitations of the hardware components.

3.1 Overcurrent protection for battery

Since the peak power of the PV installation is higher than the power capacity of the battery, a battery power limitation had to be implemented to avoid excess battery current when the PV production is high and the load consumption low. The same issue can occur the other way around, in case of high load consumption and low PV production.

Indeed, since the battery converter is regulating the DC bus voltage, it is completely transparent in terms of power flow. The powers flowing inside the DC grid are a result of the balance between production and consumption, and the controlled grid power.

To avoid reaching the battery physical power capacity, an additional protection controller was developed. For that purpose, a correction factor of the grid controlled power is generated by a set of two PI controllers. The topology of the controller is presented in Figure 8.

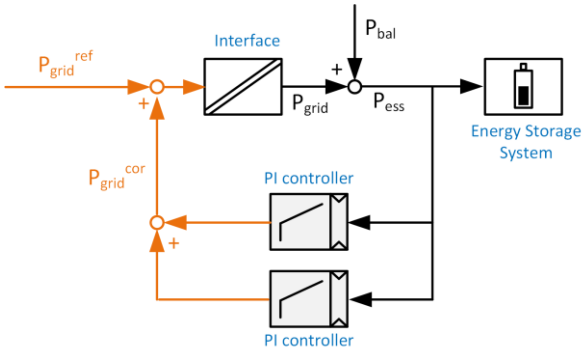

Figure 8: Protection controller to prevent battery overcurrent in charge or discharge.

In this topology, one PI controller is dedicated to limiting the battery charging current and the other is dedicated to limit the discharging one. Both include output saturation in order to avoid cross interference. The tuning of the controller has been done following the Ziegler–Nichols method.

In Figure 9, measurements of the power limitation of the charging controller is illustrated. This represents a situation with high PV production and no load consumption. The SoC being in the "self-consumption area", the grid power is supposed to be zero. However, since the power balance is exceeding the maximum power capacity of the battery (3.6 kW), this power is limited by injecting the excess in the grid.

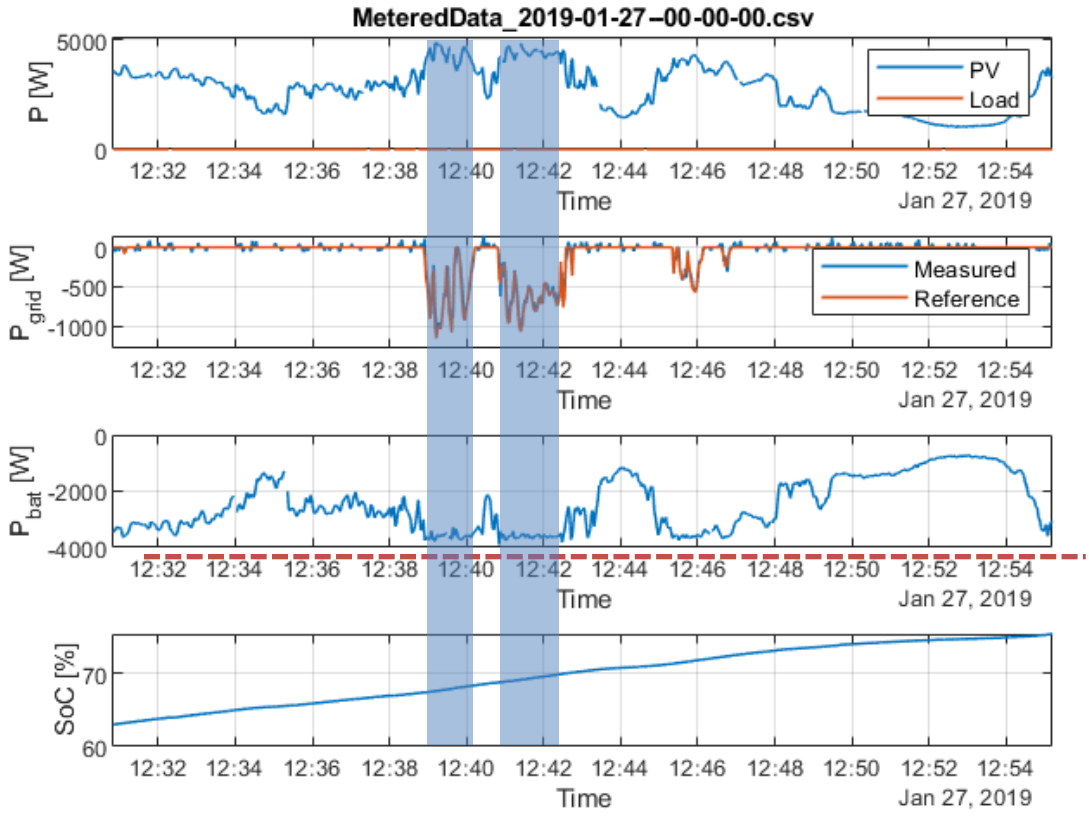

Figure 9: Evolution of PV generation, load, grid and battery power and battery SoC in a situation of high power imbalance where the battery charging power reaches its upper limit (blue highlights).

3.2 DC bus voltage regulation

In our control architecture the DC bus voltage, regulated by the battery converter, is set proportional the battery SoC (see Figure 10).

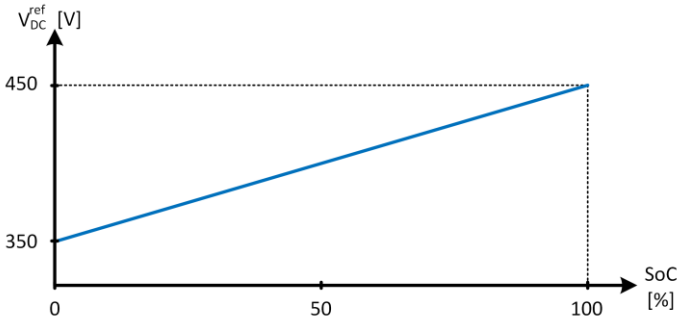

Figure 10: Relation between the reference voltage on the DC bus and the state of charge of the battery.

However, when testing the system in the laboratory prior to its installation on site, we observed that the converter was unable to properly regulate the DC voltage when charging or discharging the charging. When the battery was charging the DC bus voltage increased above the set-point, and when it was discharging the DC bus voltage decreased below the set-point.

The reason for this unwanted behaviour is that the device-level current controller of the DC/DC bidirectional converter is a proportional controller (Figure 11). Therefore, a current is flowing into/from the battery only when an error between the DC bus voltage reference (V_{DC}^{ref}) and the measured one (V_{DC}^{meas}) is observed.

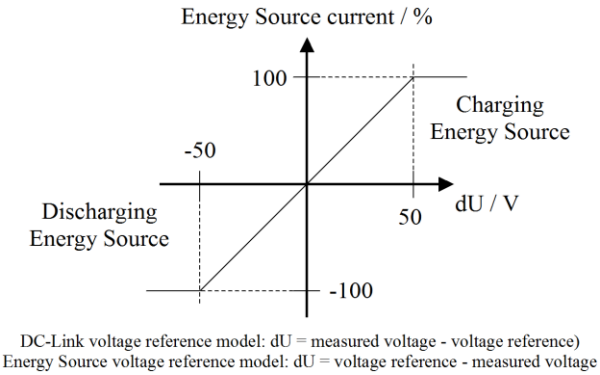

Figure 11: Device-level control of the DC/DC bidirectional converter (source: MSc Electronics Oy)

To work around this limitation, we developed an additional PI controller which determines an offset to be applied on the set-point for the DC bus voltage (Figure 12)

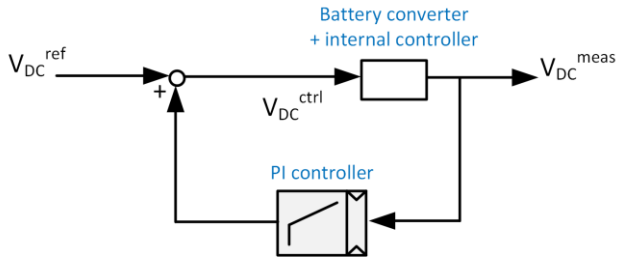

Figure 12: Additional PI controller to compensate the limitations of the battery converter.

With this correction, a regulation of the voltage can be achieved (Figure 13). In this experiment, the grid converter was controlled in order to charge and discharge the battery with a varying power.

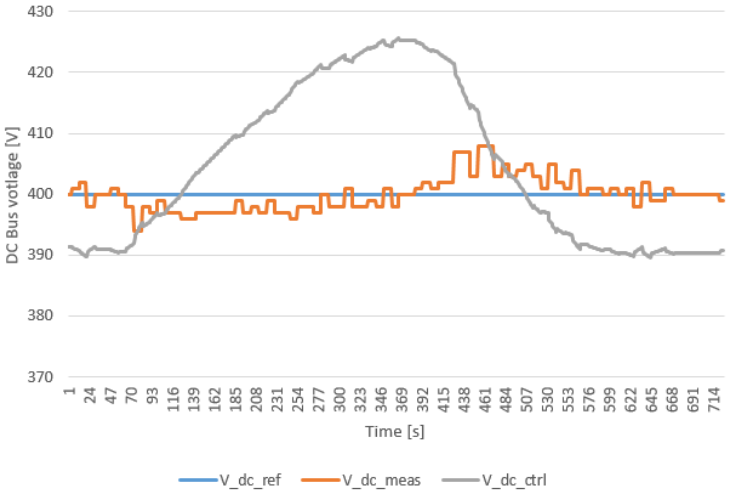

Figure 13: Validation of the additional PI controller; evolution of the "true" reference voltage for the bus (V_dc_bus), of the corrected reference voltage provided to the battery converter (V_dc_ctrl), and of the measured voltage on the DC bus (V_dc_meas).

3.3 SoC resolution issue

In the first laboratory tests, we observed extremely large set-points for the grid power when the battery SoC reached "peak-shaving areas" (E_2 or E_4 thresholds).

The reason for that behaviour turned out to be an excessive discretisation of the battery SoC, which is the main input for the control. Indeed the battery management system (BMS) of the BYD battery provides the SoC with a resolution of 1 percentage point. As a

result, the minimum non-zero error on seen by the PI controllers is 1% of the full capacity, which results in a huge control signal. Therefore a higher SoC resolution is needed in order to have a smooth control of the grid power set-point.

The solution we implemented was to use the information of battery current and voltage provided by the BMS to compute the SoC with a higher resolution. The battery power ($P_{bat} = V_{bat} \times I_{bat}$) is integrated and scaled by a factor K calculated experimentally ($\Delta SoC = \int_t K P_{bat} dt$). This integration is used to compute the fractional part of the SoC to the second decimal, and is limited to [0.00 – 0.99]. As soon as the value provided by the BMS is updated, the fraction part is set to either 0.00 (if BMS SoC increases), or 0.99 (if BMS SoC decreases).

This approach was experimentally validated (Figure 13); SoC values provided by our estimator are in good agreement with those provided by the BMS at each refresh.

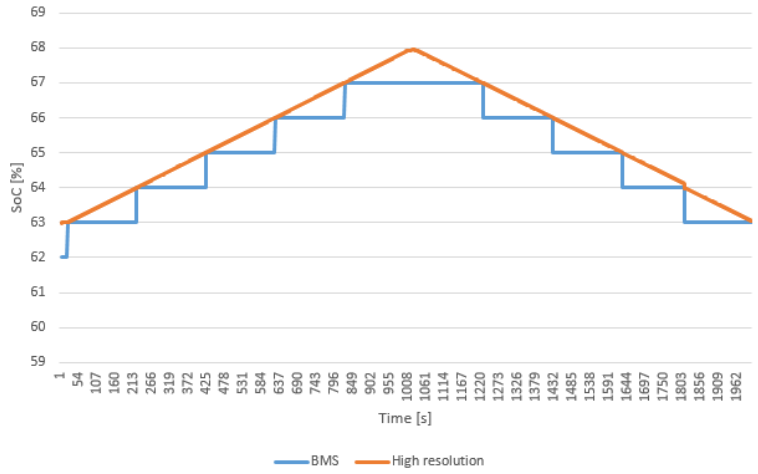

Figure 14: Evolution of the SoC provided by the BMS (blue) and corrected by integrating the battery power (orange) during a charge/discharge partial cycle at constant current.

4. Characteristics of the demonstrator

The Swiss demonstrator is operating in an industrial environment, in the wastewater treatment plant of the city of Neuchâtel. Its general structure is shown on Figure 15.

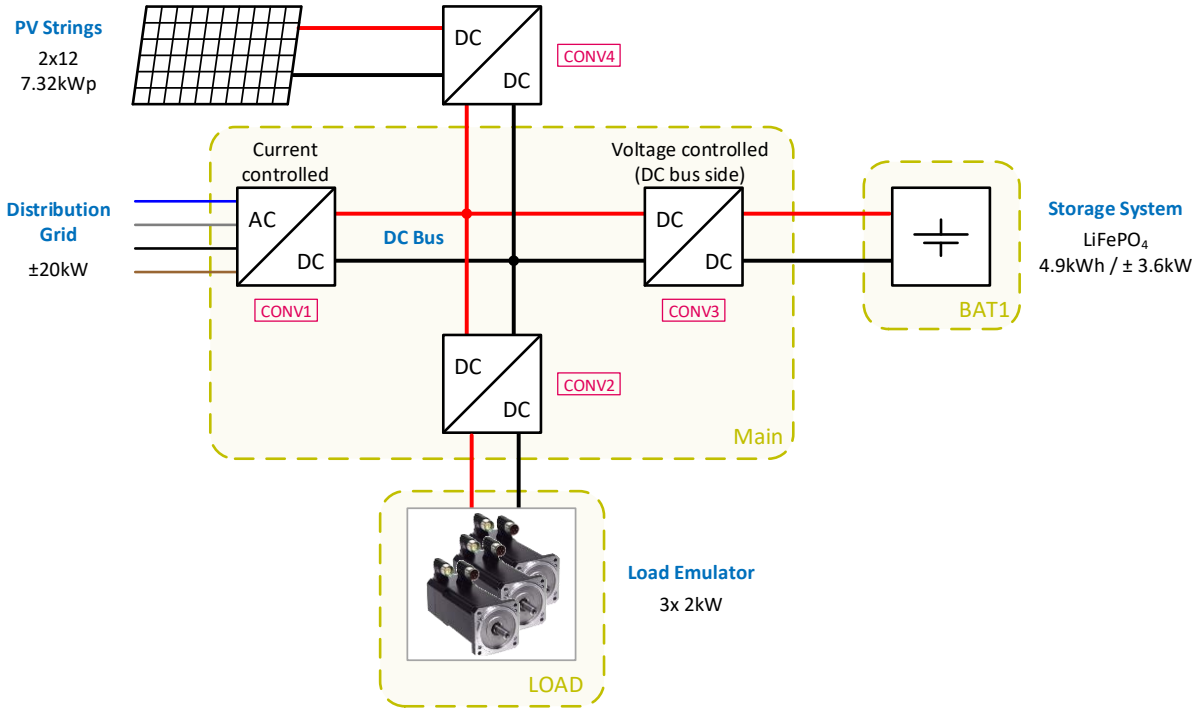

Figure 15: Components of the Swiss demonstrator.

Its main components are shown on Figure 16. They are:

- Main cabinet:
    - CONV1: A single bidirectional AC/DC converter the role of which is to interface the DC micro-grid with the up-stream AC low voltage distribution grid. This converter is linked to a local controller in order to compute volt-age, current, and power set-points. The DC side of this grid-tied converter is the common DC-link to which all the micro-grid elements are connected.
    - A central control unit, the roles of which are the system supervision and the transmission of set-points to the different local controllers.
    - CONV2: DC/DC converter supplying both the loads with adequate voltage.
    - CONV3: DC/DC converter interfacing the battery stor-age system
    - Smart-meters connected to each of the different feed-ers. Their measurements are gathered and stored in the central control unit.
- A photovoltaic system with string-level power optimizer (CONV4).
- A separate cabinet for the battery storage system.

Figure 16: Battery storage cabinet (left) and main electrical cabinet (right) of the demonstrator in operation on the Swiss demonstration site.

The loads in the demonstrator (Figure 17) comprise three distinct subsystems made of drives, brushless DC motors and magnetic powder breakers supplied by a common, insulated DC/DC converter.

Figure 17: Loads (DC-driven industrial motors) of the demonstrator.

5. Data acquisition

Figure 18 illustrates the different data flows in the Swiss Demonstrator.

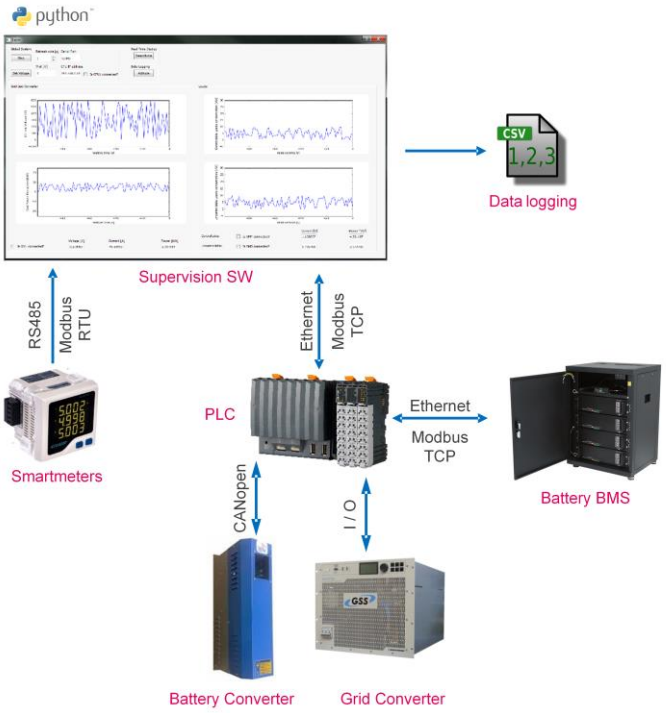

Figure 18: Data flows in the Swiss demonstrator.

All the power flows are measured by dedicated DC smart meters. These smart meters are interfaced with the central control unit, implemented on an industrial PC, through an RS-485 bus supporting a ModBus RTU communication protocol. These measurements are used only for monitoring purpose. They can be graphically displayed to the user and/or logged for further analysis with a refresh rate down to 1 second. Through this user interface (Figure 19), the user can:

- Launch the supervision system
- Start and stop the bidirectional AC/DC converter
- Monitor the state of the system: battery state of charge, set-points, internal variable of the controllers
- Visualise the temporal evolution of power flows (grid exchange, load consumption, battery charge and discharge, PV production).

For monitoring purposes it is crucial to have a reliable data collection. At first electromagnetic compatibility issues with the battery converter created significant data loss. After modification to the cables and their layout, this issue was solved and **data availability is now 99.9% with a sampling rate of 1 s.**

Figure 19: Screenshot of the graphical user interface of the Swiss demonstrator.

6. Remaining challenges

While the main features of the control strategies have all been experimentally validated, a few technical challenges remain which ideally would be solved in a commercial product.

6.1 Instability at low PV production

When the PV power production is very low (between 0 W and 200 W) the output of the string optimizer is unstable and switches off from time to time (Figure 20). This behaviour, which is common to all PV converters, creates some stress on the battery converter. Indeed, that converter produces audible oscillations at frequencies between 2 Hz and 4 Hz.

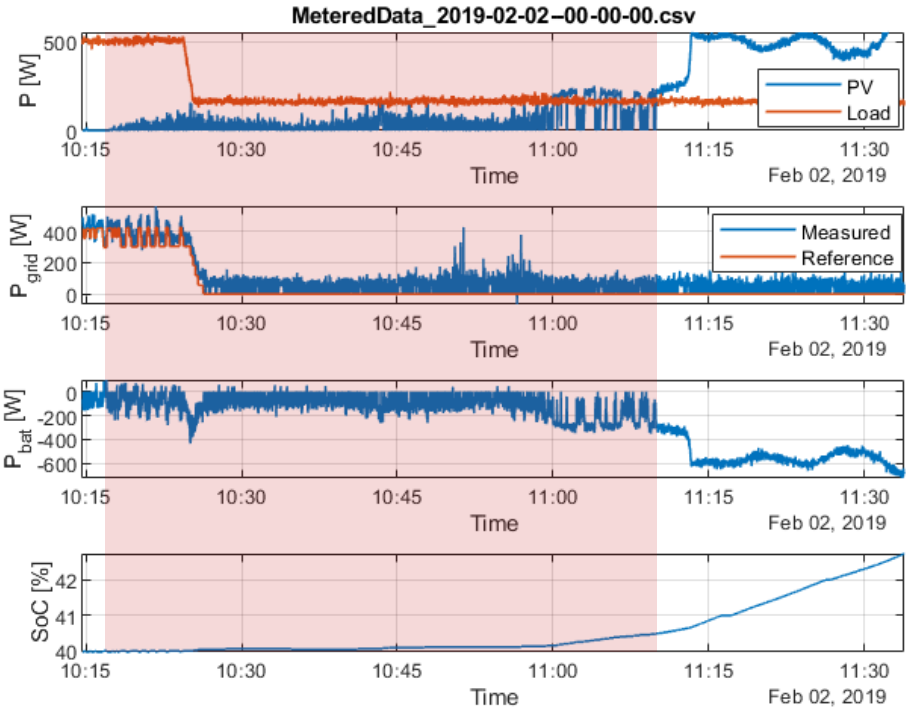

Figure 20: Rapid oscillations in power due to the string optimizer at very low PV power.

6.2 Oscillations at the E2 threshold

As shown on Figure 21, when the balance between production and consumption is constant and small and the battery is close to the boundary between two states of the system (in this case, close to the lower boundary of the self-consumption range, E2=40%), the power flows to the grid and the battery oscillate periodically. These oscillations, whose amplitude is small, are due to the discretisation of the battery SoC, which is an input to PI controllers.

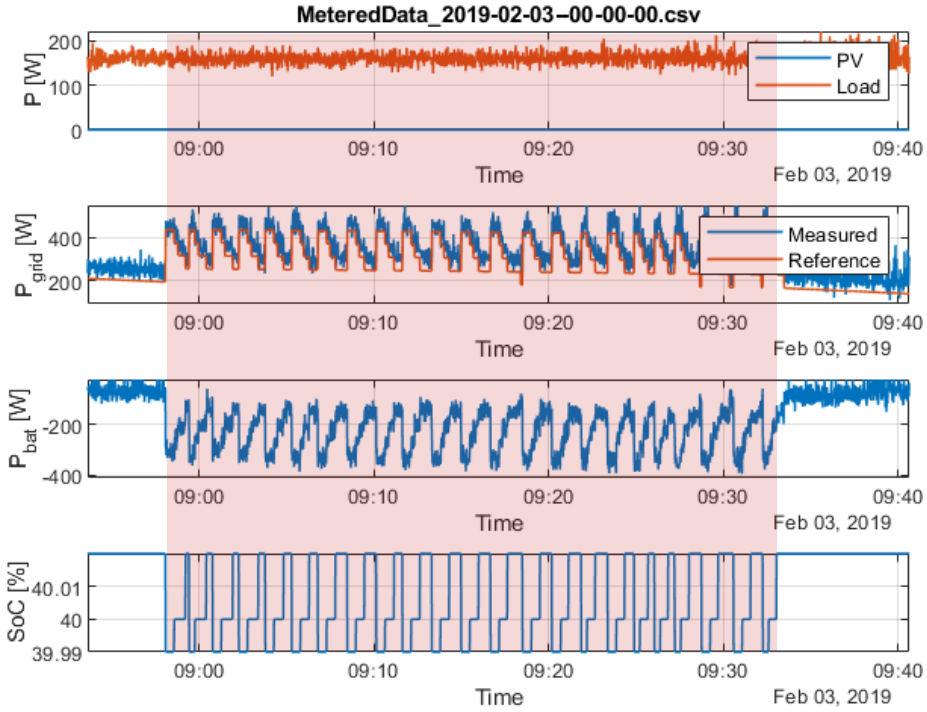

Figure 21: Oscillations in power at constant load when the battery SoC is close to threshold E2 (here: 40%)

6.3 Standby energy consumption

During the night, in the absence of PV production, the system is powered by the battery as long as its state of charge remains in the self-consumption range. When the load is also zero during the night, as is the case on Figure 22, the observed power consumption comes from the power conversion and distribution system itself. In such a situation, the decrease in SoC is 23 percentage point in 14 h. This corresponds to an energy consumption of 1.2 kWh and a continuous, standby power consumption of 84 W. The main source of this standby power consumption is the battery converter. Indeed, since it controls the DC bus voltage, it cannot be turned off at any time.

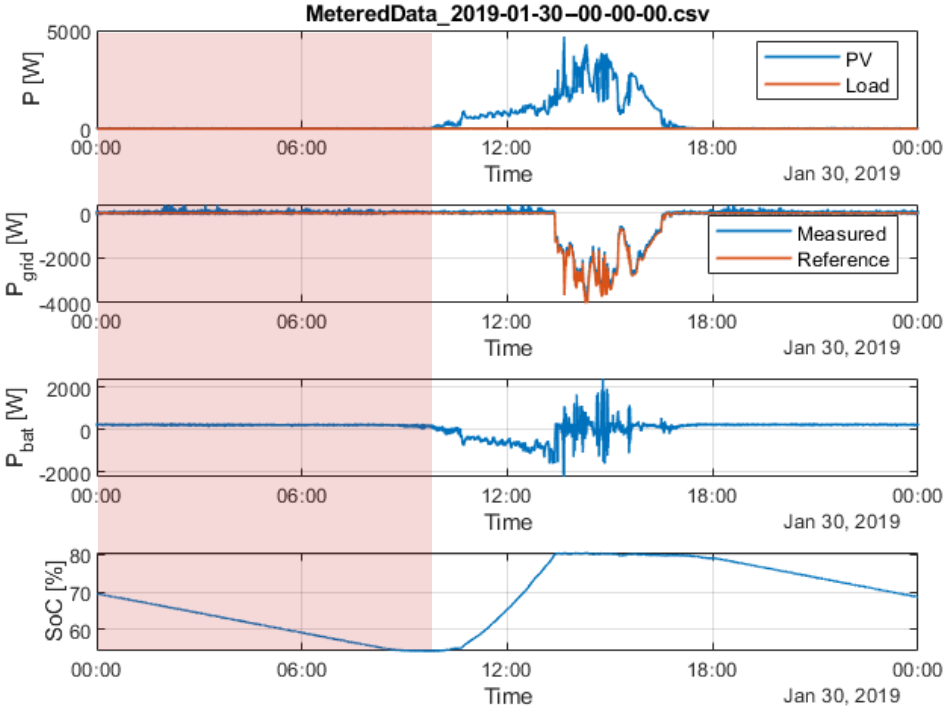

Figure 22: Evolution of power flows and battery SoC during the night, showing the standby losses of the system.

7. Results

7.1 On-site testing protocol

The demonstrator has been running on the Swiss site since December 2018. Since the loads follow an industrial schedule their profile has little day-to-day variability. Results can therefore be observed over a few days without loss of generality. Those presented in this section where acquired from the 25th to 27th January 2019. In that period the load had a square profile with 5 min, 1.8 kW spikes every 105 min.

High-level parameters for the control strategy were (Figure 23):

- E_2 = 40%
- E_4 = 80%
- $P_{lim,inj}$ = 4kW
- $P_{lim,ext}$ = 1kW / 3kW

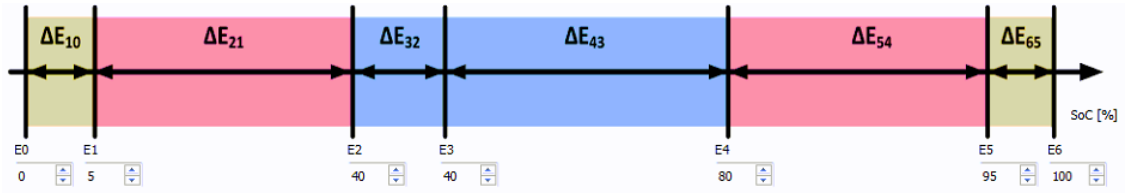

Figure 23: Distribution of the storage capacity and threshold levels applied in the period 25th to 27th January.

7.2 Overview of performance over one day

Figure 24 shows the evolution of power flows and battery SoC over a 24 h period, with the battery starting with a 50% state of charge. On that scale, the observations one can draw are:

1. The system is capable of smooth, continuous operation
2. The battery system is effectively used between 40% and 80% of its capacity to increase self-consumption by storing excess PV electricity and powering the loads.

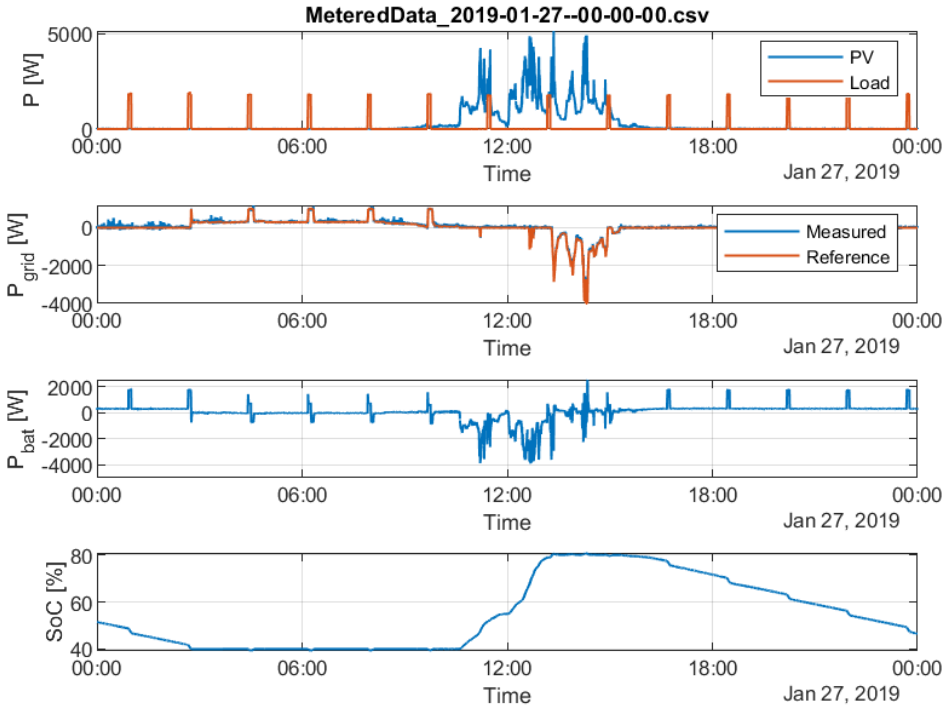

Figure 24: Evolution of PV generation, load, grid and battery power and battery SoC over 24 h.

The subsequent sections focus on validating individual parts of the control strategy.

7.3 Validation of state switching at E2 and E4

7.3.1 E2 (40% SoC)

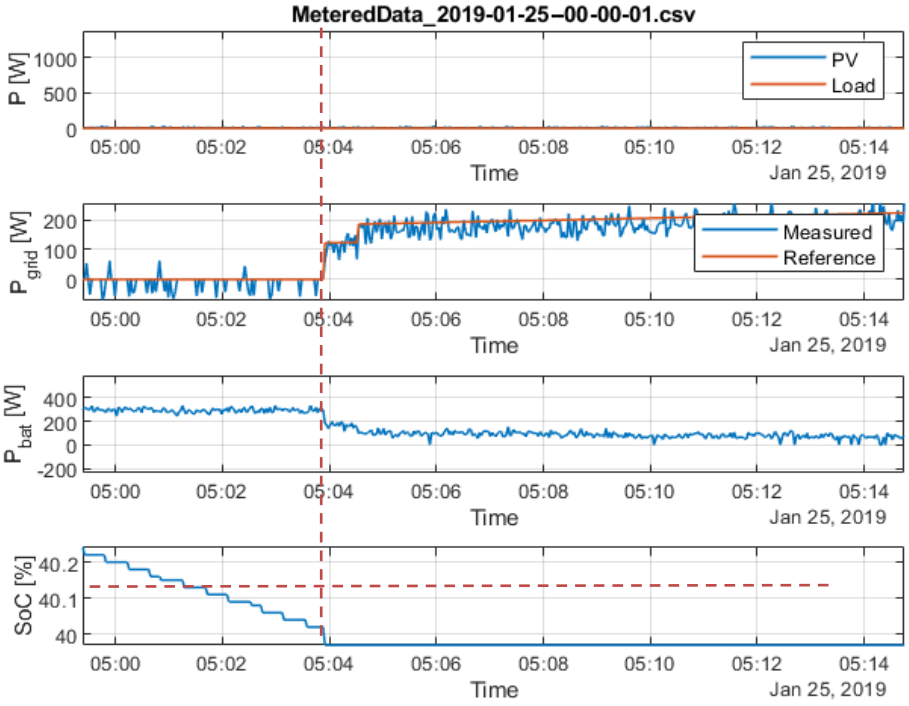

Figure 25: Evolution of power flows and SoC in the demonstrator shortly before and after the system reaching threshold E2 (40% SoC, 05:04).

Figure 25 validates the state transition in the system when it reaches threshold E2 (lower bound of the self-consumption range): at that stage the power drawn from the grid becomes non-zero and the battery power decreases.

7.3.2 E4 (80% SoC)

Symmetrically, Figure 26 validates the state transition in the system when it reaches threshold E4 (upper bound of the self-consumption range): at that stage the microgrid starts injecting power into the grid and the battery charge power decreases. On this graph the ramp-rate limitation is already clearly visible, since the transition from 0 to full PV power for the grid converter takes about 2 min 30 s.

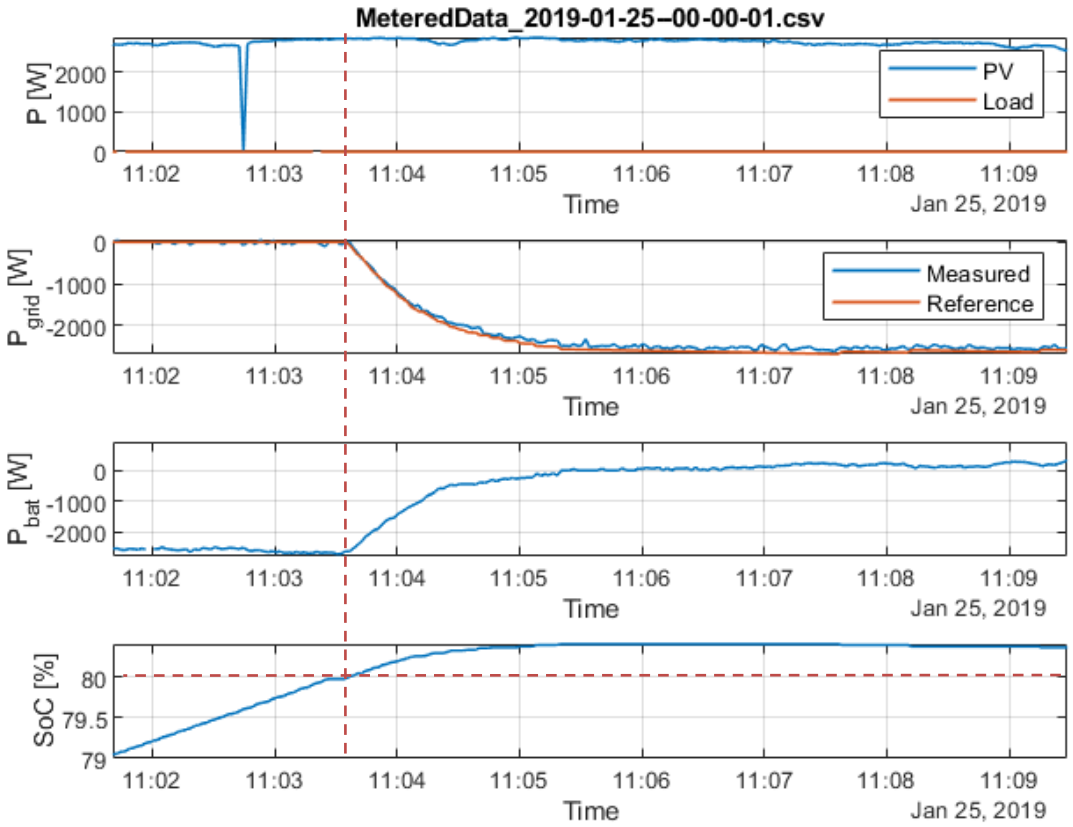

Figure 26: Evolution of power flows and SoC in the demonstrator shortly before and after the system reaching threshold E4 (80% SoC, 11:03:30).

7.4 Validation of ramp-rate control

For the validation of ramp-rate control the maximum power from the grid was set at a relatively high value (3 kW, vs. a peak power consumption of 1.8 kW). This way, the peak-shaving mode was never activated during the day, thereby isolating the ramp-rate control.

The results, illustrated on Figure 27, are in line with the expected and simulated behaviour of the system: the grid power varies smoothly and on a much longer timescale than the load (2 min 30 s to reach a new steady-state value), at the expense of the state of charge of the battery being outside the self-consumption range for a short period of time.

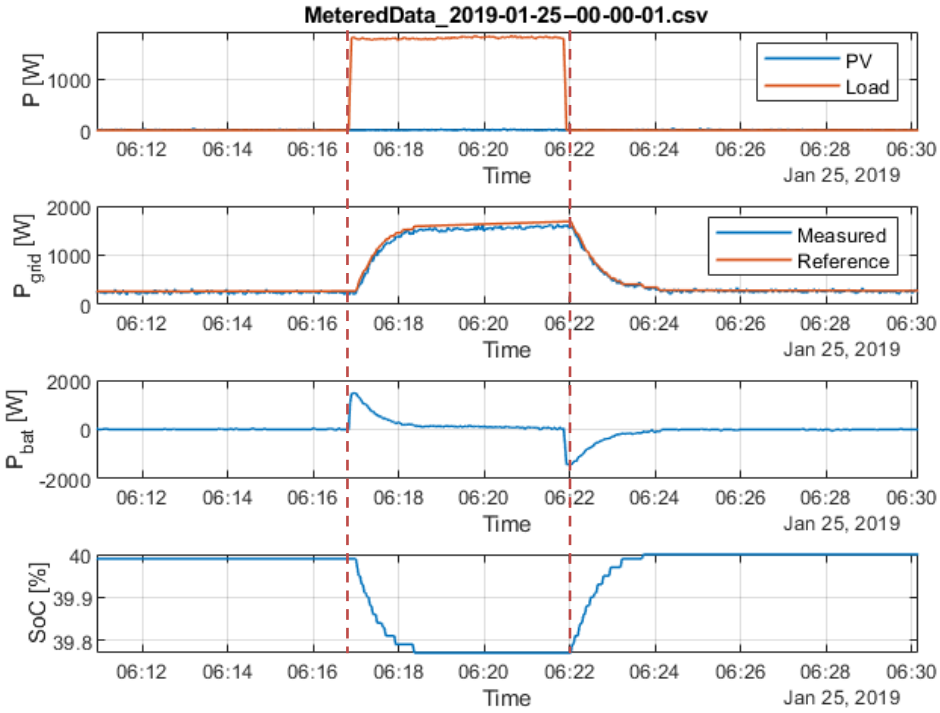

Figure 27: Evolution of power flows and SoC in the demonstrator shortly before a step increase (at about 06:16:30) and after a step decrease (at about 06:22:00) in power consumption from the load.

7.5 Validation of peak shaving

7.5.1 Power drawn from the grid

For that experiment the maximum power drawn from the grid was set at a low value (1 kW vs. a peak power consumption of 1.8 kW) on the power exchanged with the grid.

The results, shown on Figure 28, match the expectations and the simulations: the power from the grid slowly increased until reaching its limit value, the battery SoC went relatively far from the E2 threshold into the peak-shaving range, and it went back to this threshold after the peak-shaving event.

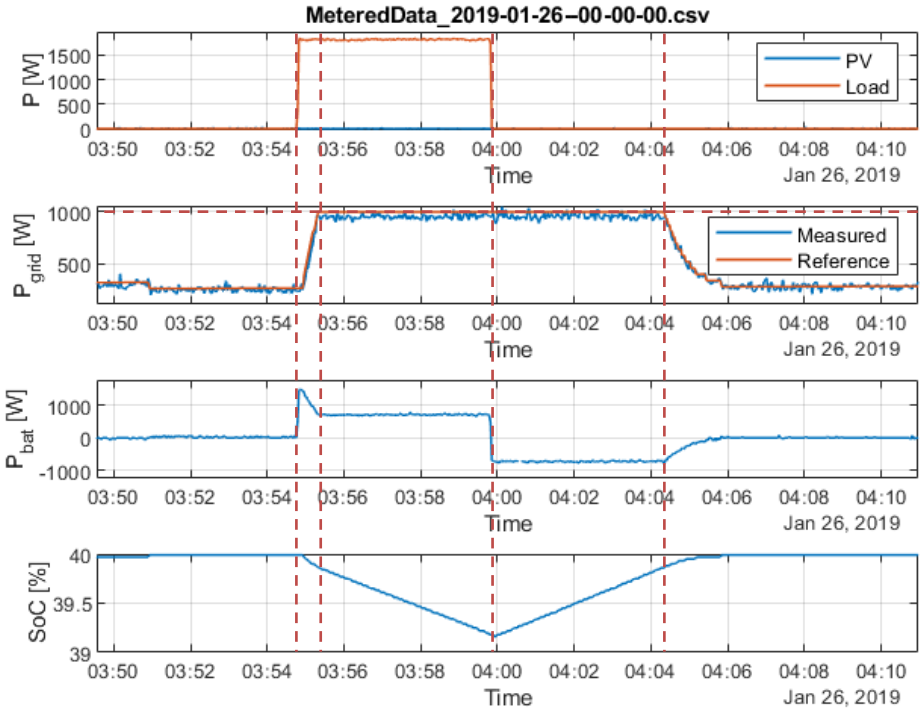

Figure 28: Evolution of power flows and battery SoC around a peak consumption event (03:54:30 to 04:00:00). When the power consumption peak starts (first vertical dashed line), the battery discharge current shoots up; in parallel, the power drawn from the grid increases only slowly due to the ramp-rate limitation mechanism. When it reaches its upper limit (here set a 1 kW, horizontal dashed line) it saturates and the battery keeps discharging to make up for the difference between the limit and the actual power consumption. When the power consumption from the load drops (third vertical dashed line) the power drawn from the grid remains constant while the battery recharges to get back near the E2 threshold. From the fourth vertical dashed line onwards the power drawn from the grid slowly decreases so that it becomes zero when the state of charge reaches the E2 threshold (lower bound of the self-consumption range) again.

7.5.2 Power injection into the grid

That validation can only be conducted on a day of relatively high PV production. In that case, the limit for power injection was set at 4 kW i.e., about half the peak power capacity of the PV system.

The results are shown on Figure 29 and validate the expected behaviour. Indeed, the injected power into the grid saturated at the set limit value of 4 kW. In addition, the smoothing effect of the ramp-rate control mechanism is visible both before the peak production, when the PV output showed rapid fluctuations, and after, when the injected power slowly went down to the new, near-steady-state value of about 1.2 kW. Finally, the battery SoC went significantly above the E4 threshold (upper bound of the self-consumption range) during the peak, well into the peak-shaving range, and went back to E4 after the peak production event.

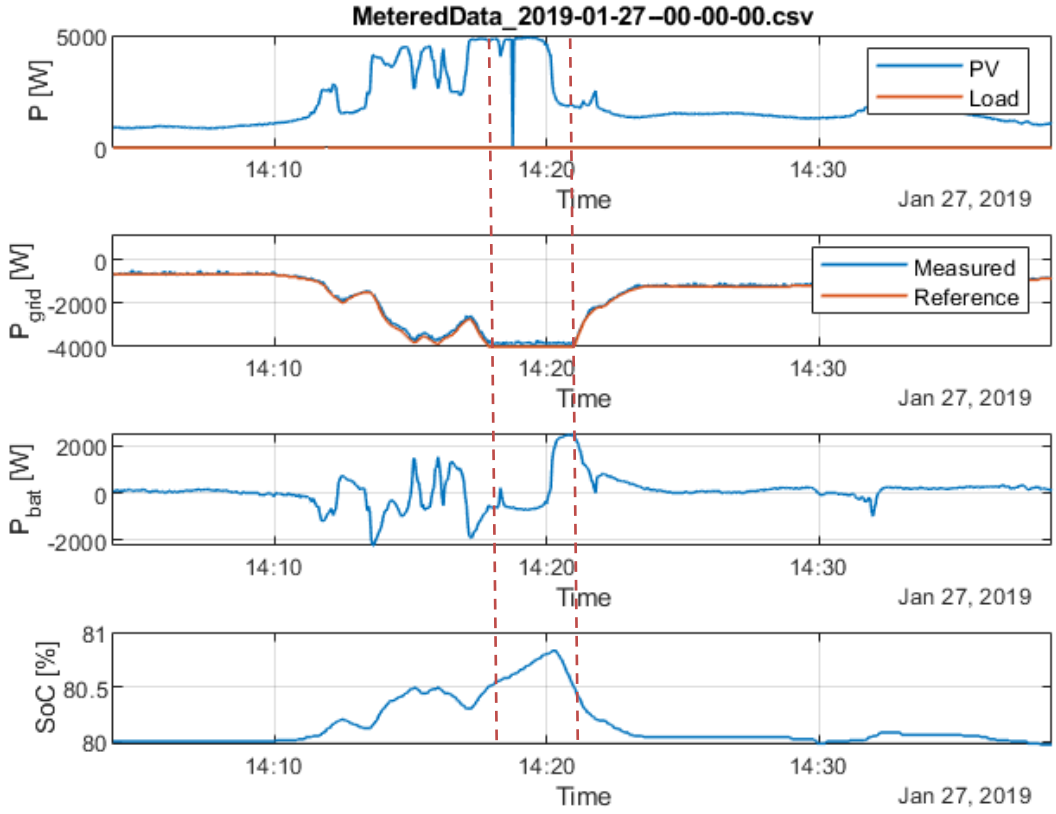

Figure 29: Evolution of power flows and battery SoC around a peak injection event. In the section before the first vertical dashed line, the battery SoC increases beyond the E4 value (upper bound of the self-consumption range) as it is used to filter out the rapid fluctuations in PV power production from the power injected into the grid. Between the two vertical dashed lines the power injection into the grid is at its maximum value; the battery first absorbs the excess PV production, then discharges after the peak production to go back towards the E4 threshold (upper bound of the self-consumption range).

8. Conclusion

The Swiss demonstration site of the DCSMART project has been operational since December 2018, providing several months of data. Its control strategies were initially validated in simulation. Several modifications proved necessary to adapt to the physical reality of the demonstration site, in particular to adapt to the limited resolution of the battery SoC provided by the battery management system, and the limited current capability of the battery storage system. Some imperfections remain, such as a non-negligible standby power consumption (84 W) and small power oscillations in specific cases. However, the all the features designed in the system have been successfully validated, with the system behaving as expected in all cases.

The DCSMART solution implemented on the Swiss demonstration site is therefore capable of providing multiple services to the public distribution grid and to the end users (increase in self-consumption of locally-produced electricity, peak shaving, and reduction in power ramp rates). The economic gains calculated in D6.1 are therefore full achievable with this solution.